Applied Catalysis B: Environmental 205 (2017) 597–604

Contents lists available at ScienceDirect

Applied Catalysis B: Environmental

journal homepage: www.elsevier.com/locate/apcatb

Thermal stability and repartition of potassium promoter between the support and active phase in the K-$Co_{2.6}Zn_{0.4}O_4$|α-Al_2O_3 catalyst for N_2O decomposition: Crucial role of activation temperature on catalytic performance

Gabriela Grzybek*, Sylwia Wójcik, Piotr Legutko, Joanna Gryboś, Paulina Indyka, Bartosz Leszczyński, Andrzej Kotarba*, Zbigniew Sojka

Faculty of Chemistry, Jagiellonian University, Ingardena 3, 30-060 Krakow, Poland

ARTICLE INFO

Article history:
Received 27 October 2016
Received in revised form
29 December 2016
Accepted 3 January 2017
Available online 4 January 2017

Keywords:
Supported cobalt spinel
Co_3O_4
deN_2O
Alkali doping
Dispersion
Potassium stability

ABSTRACT

The effect of calcination temperature of potassium promoted cobalt spinel catalyst supported on α-alumina extrudates was investigated for understanding its diverge role in N_2O decomposition. The catalyst were thoroughly characterized by XRD, μRS, IR, XPS, X-ray μ-tomography, SEM, STEM-EDX techniques. Potassium stability and surface location were evaluated by species resolved thermal alkali desorption (SR-TAD). It was found that the potassium promoter is unevenly distributed between the spinel active phase and the support, due to different energetic stability of 2.4-2.6 eV and 1.7 eV, respectively. Strong beneficial influence of the K-dopant on the catalyst activity, observed for the catalysts calcined at 500 °C, substantially attenuated upon increasing the calcination temperature above 600 °C. It was accounted for by the migration of potassium from the support to the spinel nanocrystals (below 500 °C) and subsequent formation of potassium cobaltate overlayer (above 600 °C). Thus while the support is acting as a potassium reservoir, the spinel active phase acts as a potassium sink. The presence of the cobaltate shell around the spinel nanocrystallites was revealed by FTIR and SR-TAD techniques, and corroborated by STEM-EDX elemental mapping. The results point out that in the case of the supported cobalt spinel catalysts promoted by alkali careful selection of the proper activation conditions is crucial for their optimal performance.

1. Introduction

Amongst the major sources of the anthropogenic emission of nitrous oxide – a greenhouse gas of high global warming potential – nitric and adipic acid industries belong to the most important [1]. Whereas high concentration of N_2O in the tail gasses of the adipic acid production allowed for the development of efficient abatement technologies, N_2O removal in the case of nitric acid plants still remains a largely unsolved problem. It is caused by low concentration of nitrous oxide, low temperature of tail gasses, and the presence of NO_x, H_2O, and O_2 acting as deN_2O inhibitors [2]. Many catalytic materials have been explored for development of an efficient nitrous oxide removal from the tail gasses at economically appealing low-temperature range (below 400 °C). This issue has recently been thoroughly reviewed [3].

One of the most promising systems for catalytic N_2O removal is cobalt spinel. Substantial improvement of its catalytic performance may be achieved by bulk modification (doping with alien cations such as zinc or nickel) [4–6], spreading on a carrier to enhance the number of accessible cobalt active sites [7,8], and tuning the surface properties of Co_3O_4 with alkali promoters [9–13]. The latter effect is stronger and results in lowering the reaction temperature even by 200 °C [14], yet it can be further enhanced by the additional bulk doping with e.g. zinc [15]. A beneficial effect of alkali addition on N_2O decomposition was also observed for many other oxides [9–11,13,16,17]. Its electronic nature has been elucidated definitely [13,16,17], and accounted for by the work function tuning to optimal catalytic performance controlled by potassium addition [18]. The beneficial role of alkali was found to take place both for the N_2O dissociation step and for the oxygen recombination by facilitating the electron transfer from the catalyst to the N_2O reactant (reduction, $N_2O + e^- \rightarrow N_2 + O^-$) and back from the O^- intermediate to the catalyst (oxidation, $O^- \rightarrow ½\ O_2 + e–$) [19].

Supported cobalt spinel catalysts include inert (Al_2O_3, ZrO_2, MgO) and redox active oxide carriers (CeO_2, SnO_2, TiO_2), and exhibit

* Corresponding authors.
E-mail addresses: g.grzybek@uj.edu.pl (G. Grzybek), kotarba@chemia.uj.edu.pl (A. Kotarba).

http://dx.doi.org/10.1016/j.apcatb.2017.01.005
0926-3373/

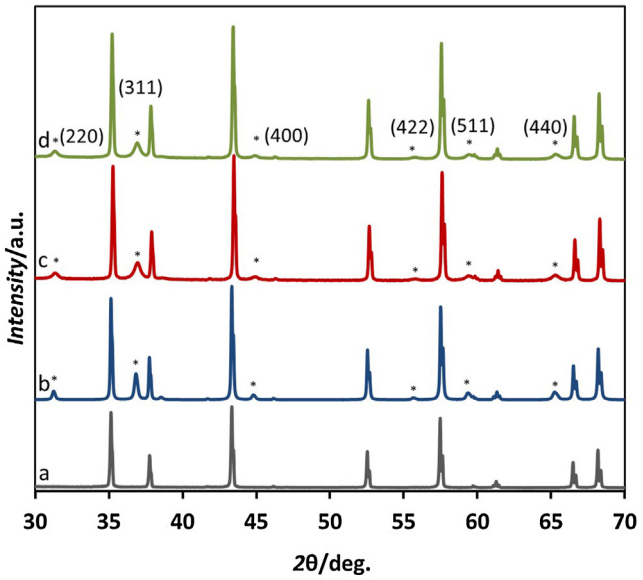

Fig. 1. Comparison of the diffraction pattern of the (a) Al_2O_3 support and K-$Co_{2.5}Zn_{0.4}$|α-Al_2O_3 catalyst calcinated at a temperature (b) 500 °C, (c) 600 °C and (d) 700 °C.

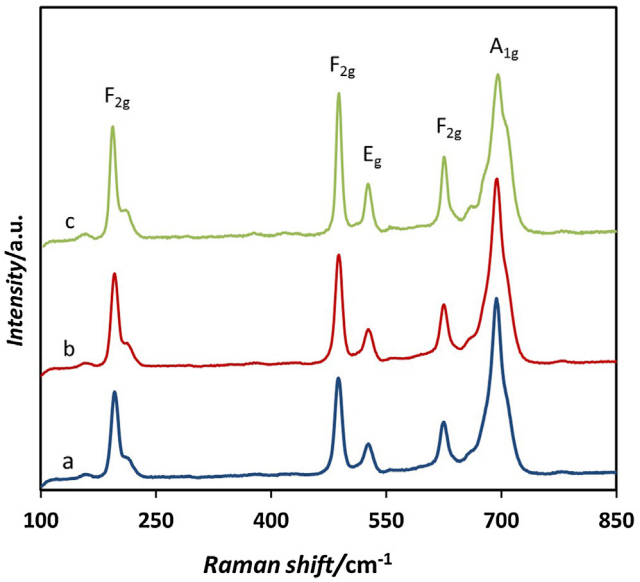

Fig. 2. Raman spectra of the K-$Zn_{0.4}Co_{2.6}O_4$|α-Al_2O_3 catalyst calcinated at temperature (a) 500 °C, (b) 600 °C and (c) 700 °C.

high deN_2O activity at much lower content of the quite expensive cobalt [3]. In the case of ceria support a synergistic effect of double redox (Co-Ce) systems was observed at the interface, but it is unfortunately lost in the presence of inhibitors [8]. The similar positive action of ceria has also been reported for CuO-CeO_2 [20].

Although several methods of various complexity are available for dispersion an active phase on a carrier, simple and effective impregnation or precipitation, which ensure enough dispersion level is the best option for industrial practice, and indeed are the most frequently applied. A ubiquitous step (unit operation) of supported catalyst preparation is calcination. It has to be carried out in the controlled conditions to assure proper dispersion of the active phase, uniform size distribution in pores of the support, and appropriate morphology. The final step of the preparation protocol is ex-situ or in-situ activation of the catalyst. It is especially important in the case of alkali promoters since they can be spread not only on the active phase but also on the support. Indeed, due to the high volatility and reactivity of the alkali promoters uncontrolled high-temperature treatment may lead to undesired processes such as surface redistribution or even a solid state reaction with the dispersed active phase, as well as promoter loss, resulting in a dramatic decrease in the catalyst performance. Although the beneficial role of alkali promoters in the N_2O decomposition is well documented, potassium surface dynamics, stability and volatility has not been examined as yet in a systematic way.

In this paper, the effect of the activation temperature on the performance of potassium promoted $Zn_{0.4}Co_{2.6}O_4$ catalyst supported on α-alumina in deN_2O reaction, and the potassium surface dynamics were investigated by means of unique species resolved thermal alkali desorption (SR-TAD) technique combined with STEM-EDX and IR, XRD, RS methods.

2. Experimental

2.1. Catalyst preparation

The α-Al_2O_3 support was prepared in the New Chemical Synthesis Institute (Pulawy, Poland) from aluminum hydroxy-oxide by calcination at 1400 °C for 4 h, and shaped into extrudes of ~2 mm in diameter and ~2 cm in length. The spinel active phase $Zn_{0.4}Co_{2.6}O_4$ was deposited on the alumina support by incipient wetness impregnation with water solution of $Co(NO_3)_2{\cdot}6H_2O$ (Sigma Aldrich, 98%), $Zn(NO_3)_2{\cdot}6H_2O$ (Sigma Aldrich, 98%) and KNO_3 (Merck KGaA, 99%), with the appropriate concentrations to obtain a spinel content of 7 wt.% and potassium content of 0.15 wt.%. Such level of alkali doping was previously found to be optimal for the K-Co_3O_4 catalyst [13]. The samples were next dried at 100 °C for 12 h, and calcined in air at 500, 600 and 700 °C for 4 h. The K-Co_3O_4 and K-α-Al_2O_3 reference samples were prepared by incipient wetness impregnation of the support with potassium nitrate solution. The reference potassium cobaltate (K_xCoO_2) was synthesized by means of ceramic synthesis from KOH and Co_3O_4 mixture, fired at 700 °C for 12 h as described in [21]. Before the proper catalytic tests the catalyst was purged in the flow of 5%N_2O/He in the temperature programmed mode (from room temperature to 600 °C) to remove the adsorbed impurity gasses, such as H_2O and CO_2, monitored by a quadruple mass spectrometer.

2.2. Characterization methods

The chemical composition of the samples was determined by means of Energy-Dispersive XRF spectrometer (Thermo Scientific, ARL QUANT'X). The X-rays of 4–50 kV (1 kV step) with the beam size of 1 mm were generated with the Rh anode. The detector used was a 3.5 mm Si(Li) drifted crystal with a Peltier cooling (~ 185 K). For quantitative analysis, the calibration with a series of metallic standards and a UniQuant software were used.

X-ray diffractograms were recorded in a Bruker D8-advance diffractometer, using CuKα radiation (λ= 1.540598 Å). The diffractograms were recorded for 2θ in the range of 10°–80° with a step of 0.02°, and a time of 3 s per step. The Raman spectra recorded at room temperature in ambient conditions were registered using a Renishaw InVia spectrometer equipped with a Leica DMLM confocal microscope and a CCD detector with an excitation wavelength of 785 nm. The Raman scattered light was collected in the spectral range of 100–800 cm^{-1} with a resolution of 1 cm^{-1}. At least five scans were accumulated to ensure a sufficient signal to noise ratio. FTIR spectra were recorded by a Nicolet 6700, Thermo Scientific spectrometer in a transmission mode with an accumulation of 124 scans. The pellets with 13 mm in diameter contained 1 mg of the sample and 100 mg of KBr.

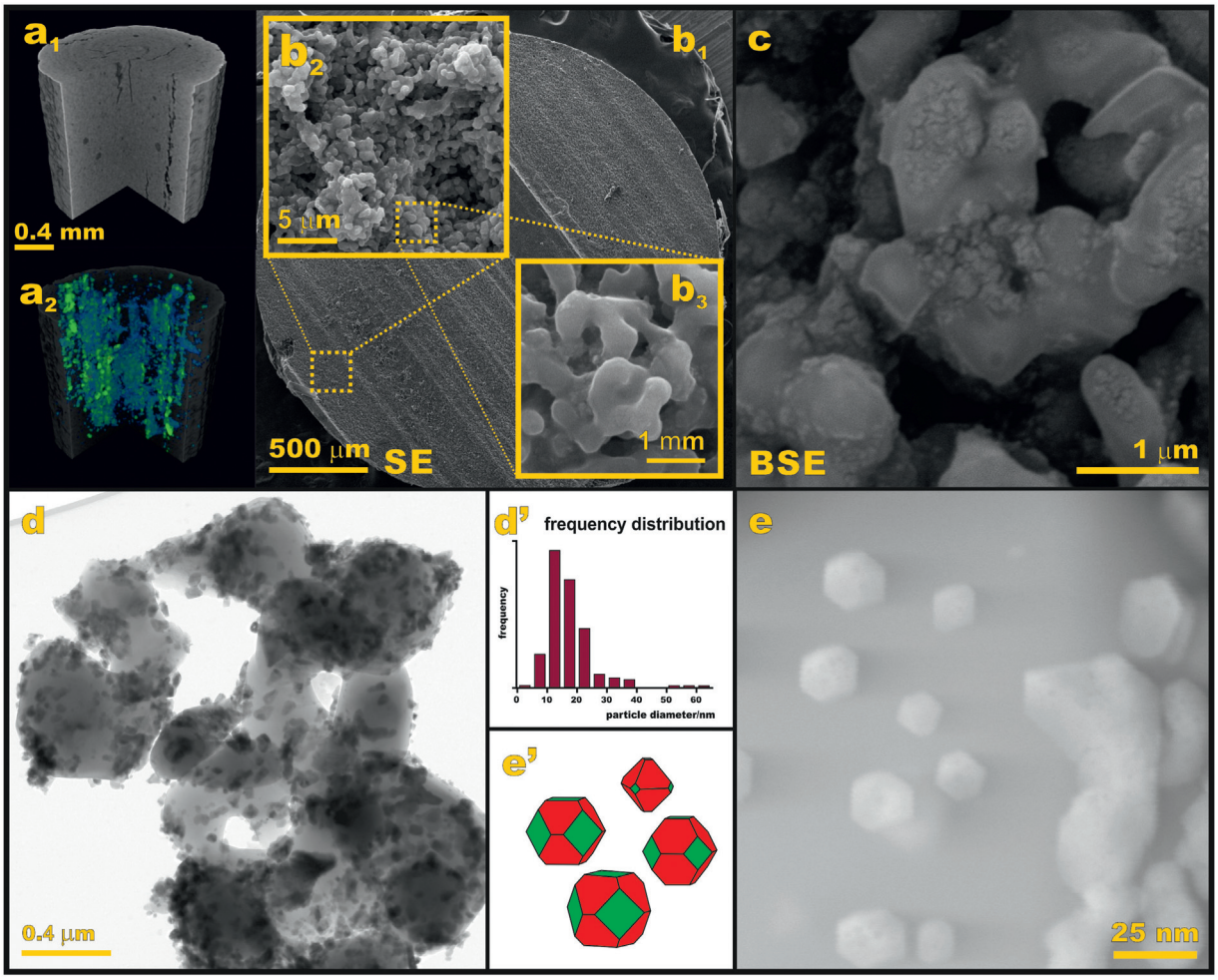

Fig. 3. Morphological and textural characterization of the K-$Zn_{0.4}Co_{2.6}O_4$|α-alumina catalyst shaped into cylindrical extrudates. (a) X-ray μ-tomographic picture of an catalyst extrudate fragment along with the corresponding porosity 3D-rendering, (b) SEM images of the extrudate cross section, and its morphology at different magnifications, (c) BSE image of the catalyst, showing the overall morphology of the spinel active phase (brighter crystallites) and the alumina carrier (darker grains), (d) BF-TEM images showing dispersion of the spinel nanocrystals over alumina micrograins (d') particle size distribution of spinel active phase, (e) STEM/HAADF pictures of the catalyst, revealing the presence of the faceted nanocrystals, (e') typical morphologies of the spinel nanocrystals retrieved by the inverse Wulff constructions.

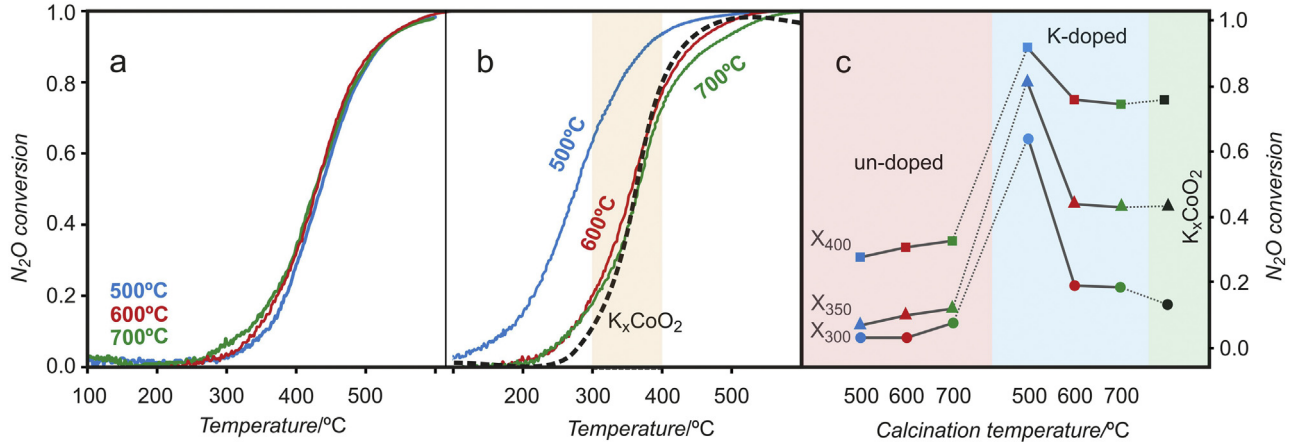

Fig. 4. The deN_2O catalytic activity of the (a) undoped and (b) K-doped catalysts and the comparison of N_2O conversion at 300, 350 and 400 °C for bare and K-doped catalysts calcined at 500, 600 and 700 °C (c).

The X-ray photoelectron spectra (XPS) were measured with a Prevac spectrometer equipped with a hemispherical VG SCIENTA R3000 analyzer. The spectra were recorded using a monochromatized AlKα source (E = 1486.6 eV), and an electron flood gun (FS40A-PS) to compensate the residual charge on the surface. The spectra were recorded with a pass energy of 100 eV for the survey and narrow scans. All the binding energies were referenced to the C 1 s peak at 285 eV of the adventitious carbon. The Tougaard-

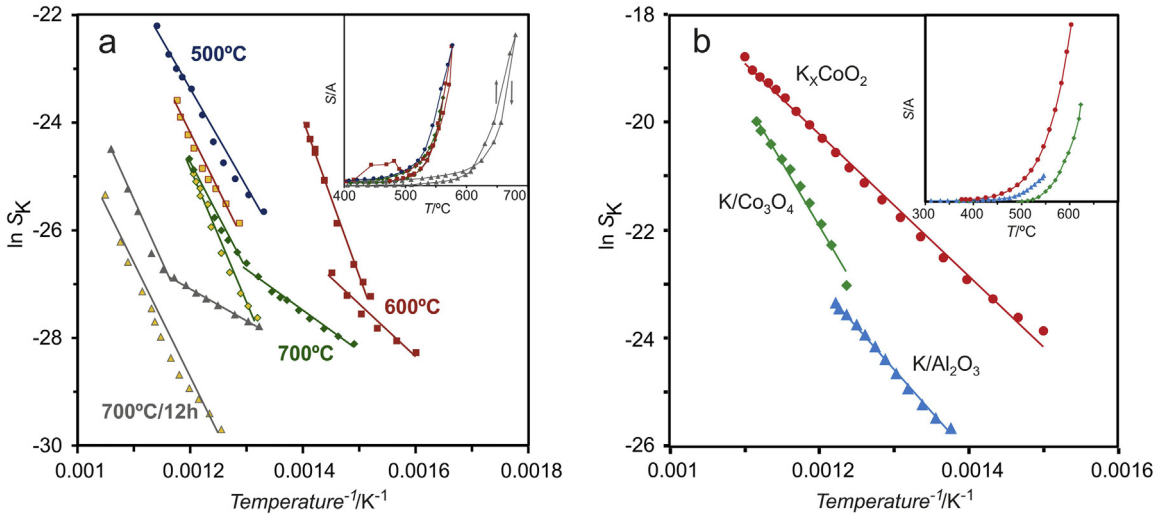

Fig. 5. Arrhenius plots of the K-desorption fluxes with the blue, red, green and grey point filling corresponding to heating and yellow to cooling of the sample together with the corresponding raw signals (inserts) for the investigated catalysts (a) and the reference samples (b). (For interpretation of the references to colour in this figure legend, the reader is referred to the web version of this article.)

Shirley and linear type baselines implemented in CasaXPS software were applied prior the analysis of the area of the photo-peaks and estimation of the integration error.

Micro-CT (micro–computed tomography) scanning was performed using the SkyScan 1172 (Kontich, Belgium) with X-ray energy of 80 keV. The pixel size was set to 1.5 μm. Prior the examination, the samples were dried at 120 °C for 2 h, and stained in 100% Lugol solution for 24 h to enhance image contrast. The specimen was scanned over 360° at 10 averaged frames per rotation step of 0.3°. Image reconstruction was performed using the NRecon software by SkyScan. For quantitative image analysis CT-Analyser software (SkyScan) was used. A 3D visualization of pores was performed using volume rendering method applied in the CTVox software.

SEM measurements were carried out on a Tescan instrument using a 20 kV acceleration voltage. The samples were gold coated prior the observations. Morphology imaging of the active phase and potassium promoter mapping was performed using a high-resolution transmission electron microscope (FEI Tecnai Osiris), equipped with an X-FEG Schottky field emitter (200 kV) and Super-X EDX (Energy Dispersive X-ray) windowless detector system with 4-sector silicon drift detector (SDD). The samples for TEM characterization were mechanically ground, then the catalysts powder was deposited on a lacey carbon-coated Cu grids. The prepared samples were loaded into a beryllium double-tilt low-background holder in order to reduce the production of spurious X-rays and transferred to the TEM microscope. The Z-contrast images were acquired using a High Angle Annular Dark Field (HAADF) detector in the scanning mode. The STEM images coupled with EDX elemental mapping were acquired with applied sample drift correction using Bruker Esprit software in order to investigate the spatial distribution of the constituent elements within the sample.

The thermal stability of potassium in the synthesized supported catalysts was investigated by species resolved thermal alkali desorption method [22]. The experiments were carried out in a vacuum apparatus with a background pressure of 10^{-8} mbar. The samples, in the form of wafers of 13 mm in diameter with a mass of about 100 mg, were heated from 200 to 650 °C in the stepwise mode at the rate of 10 °C/min. The potassium atoms (K^0) desorption fluxes were registered by means of a surface ionization detector. For each catalyst the desorption fluxes were measured during the heating and cooling of the samples. Each experimental point was averaged from about 200 measurements. The activation energy of potassium desorption was determined from Arrhenius plot (ln(signal) = f(1/*T*)) [23,24].

2.3. Catalytic tests

The Temperature Programmed Surface Reaction (TPSR) studies of N_2O decomposition were performed in a quartz flow reactor in the range of 20–600 °C (10 deg/min), using 300 mg of the catalyst (sieve fraction of 0.2–0.3 mm) with a flow rate of the feed (5% N_2O in He) of 7000 h^{-1}. The reaction progress was monitored with a quadruple mass spectrometer (RGA200, SRS, lines for m/z = 44, 32, 28, 30, 18).

3. Results and discussion

3.1. Characterization of the synthesized catalysts

The synthesized catalysts and the reference samples were thoroughly characterized with respect to their chemical composition, morphology, and texture by spectroscopic and microscopic techniques. The results of the elemental composition based on XRF analysis of the investigated samples confirmed that the content of the spinel active phase of 6.6 ± 0.3%wt. and the K promoter of 0.15 ± 0.1%wt. reflect well the desired loadings.

The crystalline structure of the prepared catalyst was studied by XRD and Raman spectroscopy. The X-ray diffraction pattern of the bare support and supported spinel catalyst are shown in Fig. 1. The diffraction peaks at 2Θ = 35.1; 37.7; 43.4; 52.5; 57.5; 59.4; 61.2; 66.5; 68.2 were indexed within a trigonal structure space group (R-3c) of α-Al_2O_3 and correspond to (104), (110), (113), (024), (116), (211), (122), (214) and (300) reflections, respectively (ICSD – 9771) [25]. In the diffractogram of the supported spinel catalyst (Fig. 1, b-d lines), apart from the dominant diffraction peaks due to the α-Al_2O_3 carrier several new diffraction lines at 2Θ = 31.3; 36.9; 44.9; 55.7; 59.5; 65.4, corresponding to (220), (311), (400), (422), (511) and (440) planes of the cobalt spinel phase, are clearly visible. The diffractograms recorded after the calcination at 500, 600, 700 °C are essentially unchanged, indicating that the overall phase structure and crystallinity of the catalyst remained intact upon such treatment.

The XRD phase analysis was supported by Raman spectroscopy. Five bands typical of the spinel structure located at 195 (F_{2g}), 487 (E_g), 526, 624 (F_{2g}) and 694 (A_{1g}) cm^{-1}, were observed (Fig. 2), confirming the presence of a nanocrystalline spinel [26–28]. The observed asymmetry of the RS peaks results from the substitution of zinc into the structure of Co_3O_4 [29]. As a result, analysis of the XRD and RS data eliminates a possibility of any ZnO segregation from the spinel phase.

The results of the multiscale morphological and textural characterization of the K-$Zn_{0.4}Co_{2.6}O_4$|α-alumina catalyst shaped into cylindrical 2 mm x 20 mm extrudates are collated in Fig. 3. An X-ray μ-tomographic picture of the extrudate fragment together with a 3D visualization of the network of micropores are shown in panels a_1, a_2, respectively. It is readily visible that the pores of the diameter in a range of 1–5 μm tend to be aligned vertically. Main pore-size fraction rendered in green corresponds to 30–40 μm. Another significant pore range consists of smaller micropores of ~3 μm in diameter, marked in blue. The overall microporosity, calculated as the ratio of the total volume of pore space to the whole sample volume, was equal to 2.52%. It corresponds to the porosity of 0.24 cm^3/g determined by water immersion method.

The alumina support grains (panel b_1–b_3), revealed by more detailed SEM measurements, exhibit an irregular rounded shape of ~0.5–2 μm in size. They are joined by well-developed necks due to sintering at 1400 °C, forming compact agglomerates. As a result, the observed micro-porosity arises from the intergranular voids. The overall morphology in a micrometric scale of the spinel and alumina grains is shown in panel (c). More detailed inspection of the catalyst nanostructure of the potassium-promoted $Zn_{0.4}Co_{2.6}O_4$|α-Al_2O_3 catalysts is provided by BF-TEM imaging (panel d). It shows that the spinel active phase is well dispersed over the alumina carrier, and the average size of the zinc-cobalt spinel crystallites is in a range of 10–20 nm, with a narrow log-normal particle size distribution (d'). The faceting of the supported spinel nanocrystals is better revealed using high-angle annular dark-field STEM examination (panel e). The typical spinel crystallites exhibit polyhedral shapes with the dominant (100) and (111) terminations as revealed by the inverse Wulff construction (e').

3.2. Catalytic tests

Prior the catalytic activity screening, the synthesized catalysts were activated in the flow of N_2O in the temperature-programmed mode from room temperature to 600 °C with the heating rate of 10 °C/min. The results expressed as N_2O conversion (X_{N2O}) versus temperature, shown in Fig. 4, reveal a dramatic difference in activity between the undoped (Fig. 4a) and K-doped (Fig. 4b) catalysts that depends on the calcination temperature. Whereas for undoped samples, there is no apparent influence of the calcination temperature (all the conversion profile in Fig. 4a are essentially the same), in the case of K-doped catalysts the samples calcined at 500 °C exhibits much higher activity than the catalysts heated at 600 °C and 700 °C (Fig. 4b). This effect has important implications since it is most pronounced in the temperature window of practical relevance i.e. 300–400 °C. Therefore, for all the investigated catalysts and reference samples, the changes in N_2O conversion for 300, 350, 400 °C for the catalysts calcined at 500, 600 and 700 °C are compared in Fig. 4c. The results clearly illustrate very similar activity of the unpromoted catalyst regardless the calcination temperature. However, in the case of K-promoted catalysts the conversion at 300 °C increases dramatically from 10% to 60% for the sample calcined at 500 °C, but only to 20% for the samples calcined at 600 °C and 700 °C. This indicates that the beneficial effect of potassium promotion observed in the case of catalyst calcined at 500 °C is to a large extend lost upon increasing the calcination temperature to 600 °C or 700 °C.

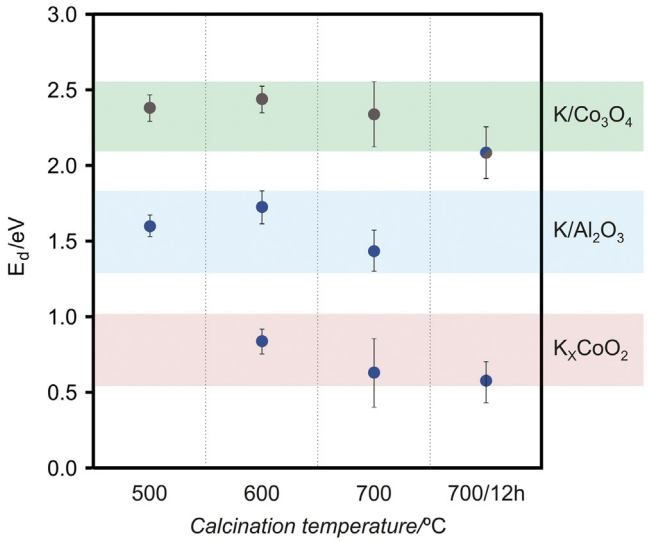

Fig. 6. The activation energy of potassium desorption for the investigated catalysts – blue points corresponds to heating and gray to cooling of the samples. Colored stripes indicate the energy ranges characteristic for three different surface potassium states: on the active spinel phase, alumina support and as a potassium cobaltate. (For interpretation of the references to colour in this figure legend, the reader is referred to the web version of this article.)

3.3. Potassium surface state

Since the promotional effect of potassium is strongly dependent on the catalyst calcination temperature it may be related to the actual potassium surface state. According to our previous studies alkali promoters are volatile at elevated temperatures [30], they may aglomerate or sperad on the catalyst surface [31], and even give rise to the formation of new surface phases by solid state reaction with both the active phase and the support [32]. Therefore, in the case of the K-$Zn_{0.4}Co_{2.6}O_4$|α-Al_2O_3 catalyst possible redistribution of potassium or formation of new phases upon calcination at higher temperature may be expected reasonably. This issue was further elucidated by means of species resolved thermal alkali desorption, IR and TEM/STEM/EDX investigations. The SR-TAD method is dedicated for studies of surface alkali dynamics by probing the temperature range of their stability, energetics of the alkali-surface bond and the alkali losses at the working temperatures.

Typical profiles of the K-desorption flux from the K-$Zn_{0.4}Co_{2.6}O_4$|α-Al_2O_3 catalysts calcined at 500, 600 and 700 °C along with the corresponding Arrhenius plots are shown in Fig. 5a. As can be seen the onset of the potassium desorption is observed at 400 °C, indicating that already at such temperature potassium becomes mobile. The exponential character of the potassium signal with the increasing temperature maybe used to determine the energy of potassium-surface bond, which is characteristic for the actual surface location of the promoter. Indeed, the Arrhenius plots ($\ln S_K$ versus $1/T$) for the catalysts calcined at 500, 600 and 700 °C exhibit different slops, revealing clear changes in the potassium surface state at each case. For attribution of the observed particular activation energies to the specific potassium state we used the SR-TAD data obtained for the model systems: K-Al_2O_3 (support), K-Co_3O_4 (active phase) and K_xCoO_2 (possible product of potassium reaction with spinel at elevated temperature), shown in Fig. 5b. These three state of potassium are characterized by distinctly different values of the K desorption activation energies (0.9, 1.4 and 2.5 eV, respectively), so they may be used reliably as a suitable benchmark for the assignment purpose. The results are summarized in a graphic way in Fig. 6. For the catalyst calcined at 500 °C the energy of 1.6 eV indicates that potassium was located mainly

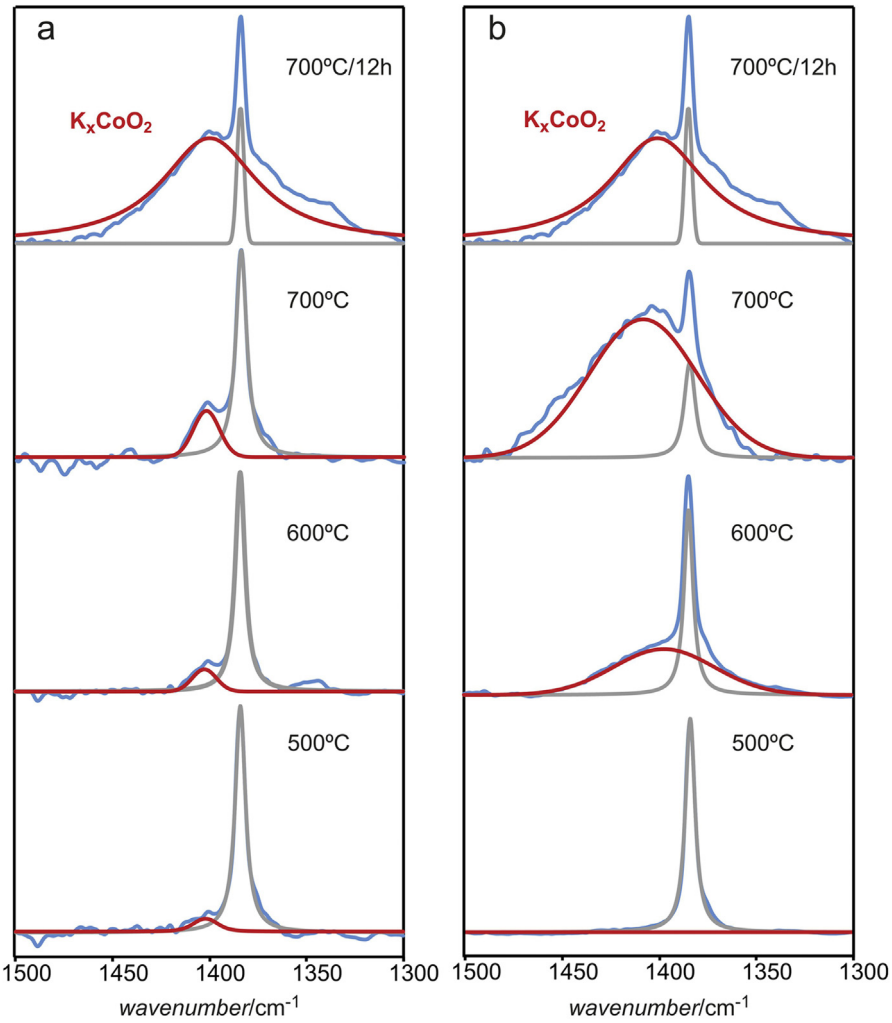

Fig. 7. FTIR spectra in the diagnostic region for the presence of K_xCoO_2 phase in the K-$Zn_{0.4}Co_{2.6}O_4$|α-Al_2O_3 catalyst calcined at different temperatures together with the associated reference (700 °C/12 h). Left panel (a) corresponds to the investigated catalysts, right panel (b) to the catalysts with the increased amount of potassium (2.5 times higher).

on the alumina support but it also decorated active phase (vide infra). Upon calcination at 600 °C, three different energy values were determined: 1.6 eV (already observed) and 2.3 eV, 0.75 eV (new ones) characteristic for potassium on the active phase and for the presence of a K_xCoO_2 phase, respectively. The analogous situation was observed for the samples calcined at 700 °C. It reveals that at temperatures above 600 °C reactivity of the potassium promoter decorating cobalt spinel is sufficient for formation of surface cobaltate phase, which is also reflected in the changes of the K-$Zn_{0.4}Co_{2.6}O_4$|α-Al_2O_3 activity (Fig. 4). Prolong calcination at 700 °C leads to the disappearance of the potassium associated with the alumina support (lack of the 1.6 eV energy in the Arrhenius plot), which implies that the potassium tends to diffuse from the support toward the active phase. The driving force for such migration is provided by the favorable stabilization energy difference between alumina and spinel, and when the calcination temperature is sufficiently high, potassium reacts with the cobalt spinel forming a undesired less reactive K_xCoO_2 layer that covers the active phase. The implied solid state reaction was next confirmed by IR studies. Preliminary survey spectra for the model K_xCoO_2 compound revealed that the region between 1300 and 1500 cm^{-1} is diagnostic for the presence of this phase.

In Fig. 7 there are two peaks observed at 1385 cm^{-1} (narrow) and 1407 cm^{-1} (broad) that correspond to surface ionic potassium species (K–O_{surf}) [33] and potassium cobaltate (K_xCoO_2). Owing to the basic character of the surface potassium species they can be revealed by IR using ambient CO_2 as a self-probe molecule (K–O_{surf} + CO_2 → K_2CO_{3surf}). In order to follow the thermal evolution of the potassium states (K–O_{surf} versus K_xCoO_2) during the calcination of the catalyst at different temperatures the experimental IR spectra (blue line in Fig. 7) were deconvoluted into the component signals of surface K_2CO_{3surf} (gray line) and bulk K_xCoO_2 (red line). In both catalyst series of two different potassium content the signal at 1385 cm^{-1} decreases, whereas that one at 1407 cm^{-1} systematically increases with the calcination temperature. These results provide a direct evidence for a clear reaction of the potassium surface K–O_{surf} species with the cobalt spinel nanocrystals leading to the progressive formation of the K_xCoO_2 cobaltate.

The redistribution of potassium upon activation at elevated temperatures was corroborated by XPS and STEM/EDX analysis. The XPS results revealed that the potassium surface concentration increases from 3.3 to 3.8 at.% upon calcination. At the same time the ratio of Co^{2+}/Co^{3+} changes from 1.35 to 1.02. Such changes are in line with the migration from the support towards active phase leading to its improved surface spreading, and strong chemical interaction with the spinel active phase which should be directly reflected in the cobalt redox alteration. However, they can also results from partial surface reduction due to oxygen release

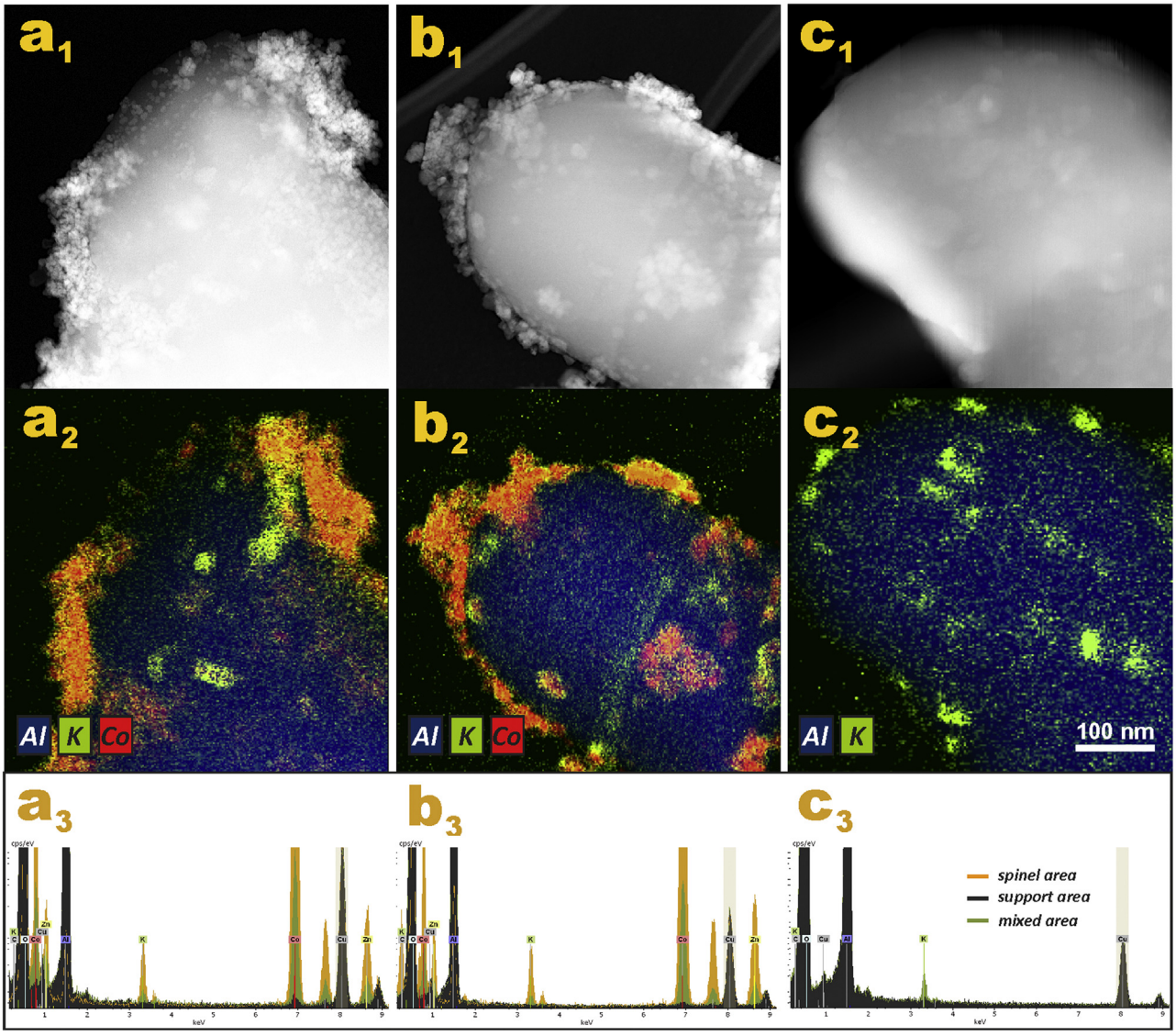

Fig. 8. STEM-HAADF images for: (a_1) K-$Zn_{0.4}Co_{2.6}O_4$|α-Al_2O_3 calcined at 500 °C, (b_1) K-$Zn_{0.4}Co_{2.6}O_4$|Al_2O_3 (600 °C), and (c_1) a reference K-α-Al_2O_3 support. HAADF Z-contrast images showing the size and distribution of the spinel nanocrystals over larger grains of α- Al_2O_3 support and nanometric potassium aggregates (clusters) spread on the catalyst. The corresponding EDX chemical maps (a2-c2) along with the associated EDX spectra (a_3-c_3) showing potassium (green) repartition between the α-Al_2O_3 support (Al in blue) and $Zn_{0.4}Co_{2.6}O_4$ spinel active phase (Co in red). (For interpretation of the references to colour in this figure legend, the reader is referred to the web version of this article.)

under heating in vacuum. Thus, to further elucidate the potassium migration the HAADF/STEM observations were performed and the obtained images of the catalyst calcined at 500 °C and 600 °C are shown in Fig. 8a_1–b_1, together with the reference K-α-Al_2O_3 sample Fig. 8c_1. The elemental maps of potassium dispersion in the investigated samples calcined at 500, 600 °C reveal apparent differences in the potassium coverage and surface location (Fig. 8a_2–c_2). The corresponding EDX source spectra (Fig. 8a_3–c_3) show that potassium signal was recorded with good signal to noise ratio, proving that the K elemental maps are reliable despite its low content in the investigated samples. While potassium in the K-$Zn_{0.4}Co_{2.6}O_4$|Al_2O_3 catalyst calcined at 500 °C resides on both the spinel and on the Al_2O_3 support, after calcination at 600 °C appreciable potassium depletion on the support and enhancement on the spinel phase can be noticed. It is worth noting here that the total abundance of potassium in all the investigated samples determined by XRF technique remains essentially the same regardless the calcination temperature. It can be thus concluded that at such conditions potassium is relocated but not lost from the catalyst surface. The alumina support may be considered as a reservoir of mobile potassium promoter.

For the catalyst calcined at 500 °C the EDX results revealed relatively uniform potassium redistribution on the Al_2O_3 support and its accumulation on the $Zn_{0.4}Co_{2.6}O_4$ spinel phase in accordance with the higher stabilization energy (1.6 vs. 2.4 eV). In the case of higher calcination temperature of 600 and 700 °C potassium enhanced migration from the support towards spinel nanocrystallites enabling for the solid state reaction to occur that results in K_xCoO_2 surface phase, as shown by the IR (Fig. 7) and SR-TAD (Fig. 6) results. The occurrence of the potassium cobaltate formation is also supported in an indirect way by the significant changes in the shape of the active phase nanocrystals (Fig. 8), while in the case of potassium free samples the calcination temperature had a negligible effect of the spinel nanocrystallites morphology.

Analysis of all the obtained spectroscopic, microscopic and K-desorption data allowed to propose a comprehensive description of the potassium status and dynamics on the supported K-$Zn_{0.4}Co_{2.6}O_4$|α-Al_2O_3 catalyst. In the case of potassium depo-

sition on the surface of the spinel phase the promotional effect strongly depends on the K coverage in a non-monotonous fashion, as showed by us elsewhere [13,34]. The maximum of the promotional effect was observed for a rather narrow doping levels in the range of 2–6 K at. nm^{-1} (0.10–0.40 wt.%). Large deviations from these values have pronounce negative impact on the catalyst activity. For supported catalysts, achievement of optimal K-doping level is not that straightforward as in the case of bulk spinels since as shown above potassium maybe distributed unevenly between the support and the active phase. The large differences in the corresponding stabilization energies provides sufficient driving force for a facile potassium surface migration. As a consequence, the calcination temperature of the K-$Zn_{0.4}Co_{2.6}O_4|Al_2O_3$ catalyst may not only influence the K surface loading on the active phase but also induce the solid state reaction between the potassium promoter and the spinel. Indeed, it has been reported that the interaction of K_2O mixed with Co_3O_4 at 600 °C leads to straightforward formation of the K_xCoO_2 cobaltate phase [35]. Its structure can be regarded as stacking of the CoO_2 slabs composed of the CoO_6 octahedra with the sharing edges, and the potassium ions randomly distributed within the interslab space. Since the slab structure of the cobaltate is similar to the parent spinel (111) layer, formation of the K_xCoO_2 phase may be regarded as expansion of the spinel (111) planes by incorporation of the mobile potassium ions provided from the support K-reservoir. The potassium incorporation level controls the Co^{3+}/Co^{4+} ratio, and significant increase in the content of the tetravalent cobalt that leads to work function enhancement, which is harmful for the deN_2O catalytic activity, as well-documented and explained elsewhere [13,14]. The surface status of potassium apart from the calcination temperature of the catalyst may also be influenced by the presence of residuals (H_2O, NO) in the real time-on-stream conditions. Indeed, previous studies on the congener K-$Co_{2.6}Zn_{0.4}O_4$ catalyst revealed that a more negative effect is due to NO, which interacting with surface potassium give rise to gradual development of KNO_{3surf} species [29].

The obtained results have also a direct practical significance, since they show that for the supported spinel catalyst two interconnected preparation parameters: potassium surface loading and calcination temperature are of crucial importance. For the optimization of the promotional effect of potassium they should be carefully adjusted and controlled to assure the desired and stable K coverage over the spinel phase during the catalyst formation and operation. This study may also explain a large range of the N_2O conversion values reported for nominally the same cobalt spinel [18], since it is quite likely that the actual level of alkali content and the calcination temperature were not always controlled on purpose.

4. Conclusions

The effect of calcination temperature on the potassium stability and its surface location on the K-$Zn_{0.4}Co_{2.6}O_4|Al_2O_3$ catalyst for N_2O decomposition was investigated by XRD, RS, IR, X-ray μ-tomography, SEM, STEM-EDX and SR-TAD techniques. It was found, that due to its different energetic stability, the potassium promoter is unevenly distributed between the spinel active phase (2.4 – 2.6 eV) and the alumina support (1.7 eV). The loss of the strong beneficial influence of the K-dopant on the catalyst activity above 600 °C was accounted for by the migration of potassium from the support (acting as K-reservoir) to the spinel nanocrystals and subsequent formation of a K_xCoO_2 overlayer. The obtained results clearly showed that the calcination at elevated temperature may influence not only the sintering of the nanocrystaline active phase but primarily the promoter surface state, leading at the limit to the new phase formation. Thus the careful selection of the activation conditions for the K-$Zn_{0.4}Co_{2.6}O_4|Al_2O_3$ catalyst is indispensable for its optimal performance. The revealed surface dynamics of potassium (mobility and reactivity with transition metal oxides) may also explain the discrepancies observed in the literature, concerning the activities of other akin supported catalysts promoted by alkali.

Acknowledgements

Authors would like to acknowledge the Polish National Centre for Research and Development funding awarded by the decision number PBS2/A5/38/2013. The research was partially carried out with the equipment purchased thanks to the financial support of the European Regional Development Fund in the framework of the Polish Innovation Economy Operational Program (contract no. POIG.02.01.00-12-023/08).

References

[1] Eurostat—the Statistical Office of the European Communities http://epp.eurostat.ec.europa.eu.
[2] J. Pérez-Ramírez, F. Kapteijn, K. Schöffel, J.A. Moulijn, Appl. Catal. B 44 (2003) 117.
[3] Michalis Konsolakis, ACS Catal. 5 (2015) 6397.
[4] L. Yan, T. Ren, X. i Wang, Q. Gao, D. Ji, J. Suo, Catal. Commun. 4 (2003) 505.
[5] N. Russo, D. Fino, G. Saracco, V. Specchia, Catal. Today 119 (2007) 228.
[6] L. Yan, T. Ren, X. Wang, D. Ji, J. Suo, Appl. Catal. B 45 (2003) 85.
[7] Q. Shen, L. Li, J. Li, H. Tian, Z. Hao, J. Hazard. Mater. 163 (2009) 1332.
[8] G. Grzybek, P. Stelmachowski, S. Gudyka, P. Indyka, Z. Sojka, N. Guillén-Hurtado, V. Rico-Pérez, A. Bueno-López, A. Kotarba, Appl. Catal. B 180 (2016) 622.
[9] C. Ohnishi, K. Asano, S. Iwamoto, K. Chikama, M. Inoue, Catal. Today 120 (2007) 154.
[10] K. Asano, C. Ohnishi, S. Iwamoto, Y. Shioya, M. Inoue, Appl. Catal. B 78 (2008) 242.
[11] N. Pasha, N. Lingaiah, N.S. Babu, P.S.S. Reddy, P.S.S. Prasad, Catal. Commun 10 (2008) 132.
[12] L. Xue, Ch. Zhang, H. He, Y. Teraoka, Catal. Today 126 (2007) 449.
[13] F. Zasada, P. Stelmachowski, G. Maniak, J.-F. Paul, A. Kotarba, Z. Sojka, Catal. Lett. 127 (2009) 126.
[14] P. Stelmachowski, G. Maniak, A. Kotarba, Z. Sojka, Catal. Commun. 10 (2009) 1062.
[15] P. Stelmachowski, F. Zasada, G. Maniak, P. Granger, M. Inger, M. Wilk, A. Kotarba, Z. Sojka, Catal. Lett. 130 (2009) 637.
[16] N. Pasha, N. Lingaiah, P.S.S. Reddy, P.S.S. Prasad, Catal. Lett. 118 (2007) 64.
[17] N. Pasha, N. Lingaiah, P.S.S. Reddy, P.S.S. Prasad, Catal. Lett. 127 (2009) 101.
[18] W. Piskorz, F. Zasada, P. Stelmachowski, A. Kotarba, Z. Sojka, Catal. Today 137 (2008) 418.
[19] G. Grzybek, P. Stelmachowski, S. Gudyka, J. Duch, K. Ćmil, A. Kotarba, Z. Sojka, Appl. Catal. B 168–169 (2015) 509.
[20] M.N. Moreira, A.M. Ribeiro, A.F. Cunha, A.E. Rodrigues, M. Zabilskiy, P. Djinović, A. Pintar, Appl. Catal. B 189 (2016) 199.
[21] T. Jakubek, W. Kaspera, P. Legutko, P. Stelmachowski, A. Kotarba, Catal. Commun. 71 (2015) 37.
[22] A. Kotarba, W. Rożek, I. Serafin, Z. Sojka, J. Catal. 247 (2007) 238.
[23] K. Engvall, L. Holmlid, A. Kotarba, J.B.C. Pettersson, P.G. Menon, P. Skaugset, Appl. Catal. A 134 (1996) 239.
[24] B. Ura, J. Trawczyński, A. Kotarba, W. Bieniasz, M.J. Illán-Gómez, A. Bueno-López, F.E. López-Suárez, Appl. Catal. B 101 (2011) 169.
[25] A. Takigawa, S. Tachibana, G.R. Huss, K. Nagashima, K. Makide, A.N. Krot, H. Nagahara, Geochim. Cosmochim. Acta 124 (2014) 309.
[26] Y. Wei, K.W. Nam, K.B. Kim, G. Chen, Solid State Ion 177 (2006) 29.
[27] L.V. Gasparov, D.B. Tanner, D.B. Romero, H. Berger, G. Margaritondo, L. Forro, Phys. Rev. B 62 (2000) 7939.
[28] Z.H. Zhou, J.M. Xue, J. Wang, H.S.O. Chan, T. Yu, Z.X. Shen, J. Appl. Phys. 91 (2002) 6015.
[29] M. Inger, M. Wilk, M. Saramok, G. Grzybek, A. Grodzka, P. Stelmachowski, W. Makowski, A. Kotarba, Z. Sojka, Ind. Eng. Chem. Res. 53 (2014) 10335.
[30] W. Bieniasz, M. Trebala, Z. Sojka, A. Kotarba, Catal. Today 154 (2010) 224.
[31] M. Trebala, W. Bieniasz, M. Drozdek, M. Molenda, A. Kotarba, Z. Sojka, Funct. Mater. Lett. 4 (2011) 179.
[32] P. Legutko, T. Jakubek, W. Kaspera, P. Stelmachowski, Z. Sojka, A. Kotarba, Catal. Commun. 43 (2014) 34.
[33] T. Montanari, L. Castoldi, L. Lietti, G. Busca, Appl. Catal. A 400 (2011) 61.
[34] P. Stelmachowski, F. Zasada, G. Maniak, P. Granger, M. Inger, M. Wilk, A. Kotarba, Z. Sojka, Catal. Lett. 130 (2009) 637.
[35] M. Blangero, R. Decourt, D. Carlier, G. Ceder, M. Pollet, J.-P. Doumerc, J. Darriet, C. Delmas, Inorg. Chem. 44 (2005) 9299.